

MSDet: Receptive Field Enhanced Multiscale Detection for Tiny Pulmonary Nodule

Guohui Cai, Ying Cai*, Zeyu Zhang, Daji Ergu, Yuanzhouhan Cao, Binbin Hu, Zhibin Liao, and Yang Zhao

Abstract—Pulmonary nodules are critical indicators for the early diagnosis of lung cancer, making their detection essential for timely treatment. However, traditional CT imaging methods suffered from cumbersome procedures, low detection rates, and poor localization accuracy. The subtle differences between pulmonary nodules and surrounding tissues in complex lung CT images, combined with repeated downsampling in feature extraction networks, often lead to missed or false detections of small nodules. Existing methods such as FPN, with its fixed feature fusion and limited receptive field, struggle to effectively overcome these issues. To address these challenges, our paper proposed three key contributions: Firstly, we proposed MSDet, a multiscale attention and receptive field network for detecting tiny pulmonary nodules. Secondly, we proposed the extended receptive domain (ERD) strategy to capture richer contextual information and reduce false positives caused by nodule occlusion. We also proposed the position channel attention mechanism (PCAM) to optimize feature learning and reduce multiscale detection errors, and designed the tiny object detection block (TODB) to enhance the detection of tiny nodules. Lastly, we conducted thorough experiments on the public LUNA16 dataset, achieving state-of-the-art performance, with an mAP improvement of 8.8% over the previous state-of-the-art method YOLOv8. These advancements significantly boosted detection accuracy and reliability, providing a more effective solution for early lung cancer diagnosis. The code will be available at <https://github.com/CaiGuoHui123/MSDet>.

Index Terms—Pulmonary nodule; Computer tomography; Tiny object detection; Hybrid CNN-Transformer;

I. INTRODUCTION

LUNG cancer remains the leading malignancy in terms of both incidence and mortality rates worldwide [1]. Pulmonary nodules are among the earliest clinical manifestations of lung cancer, underscoring the critical importance of early detection. Currently, computed tomography (CT) is the primary modality utilized by clinicians for the screening of pulmonary nodules [2], [3]. Pulmonary nodules, typically characterized as intrapulmonary spherical lesions, range in diameter from 3 to 30 mm. The complexity of the lung environment and the variability of nodule size and morphology make nodule detection difficult. At the same time, small nodules in lung CT scans are often visually difficult to distinguish

Guohui Cai, Ying Cai (*corresponding author), Daji Ergu, and Binbin Hu are with the College of Electronic and Information, Southwest Minzu University, Chengdu, China (e-mail: guohuicai123@163.com; caiying34@yeah.net; ergudaji@163.com; binhu0821@163.com).

Zeyu Zhang is with the Australian National University, Canberra ACT 2601, Australia (e-mail: steve.zeyu.zhang@outlook.com).

Yuanzhouhan Cao is with the School of Computer Science and Technology, Beijing Jiaotong University, Beijing, China (e-mail: yzhcao@bjtu.edu.cn).

Zhibin Liao is with the University of Adelaide, Adelaide, Australia (e-mail: zhibin.liao@adelaide.edu.au).

Yang Zhao is with La Trobe University, Melbourne, Australia (e-mail: y.zhao2@latrobe.edu.au).

from surrounding tissues, resulting in a high rate of missed detection or false positives.

mAP of Different Detection Models for Lung Nodule Detection

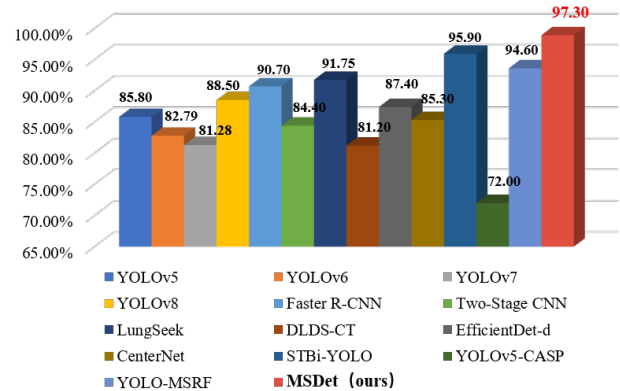


Fig. 1. Comparative histogram between the state-of-the-art network and MSDet, MSDet (Ours) achieved the best result of 97.30% in terms of pulmonary nodule detection accuracy in CT images.

Object detection methods have been widely adapted in medical imaging to automatically analyze imaging data and identify suspicious lesion areas. Two-stage detection algorithms [4]–[7] initially detect all potential nodules from CT scans, which often results in a high number of false positives. However, these networks are typically complex and time-consuming, relying on feature maps and prior knowledge (e.g., anchor frames), leading to inaccurate localization, particularly for small or variably shaped nodules. Besides, one-stage detection algorithms [8]–[14] integrate nodule candidate detection and false positive reduction into a single model, achieving higher detection speeds but struggling with small nodules and occlusions, which can result in missed detections and false positives.

Meanwhile, YOLOv5, a popular one-stage detection algorithm, offers notable advantages such as adaptive anchor box computation and improved feature fusion, which enhance its speed and spatial information processing capabilities. Hence, developed a one-stage detection method based on YOLOv5 presented to be a promising trend to address these challenges. However, YOLOv5 still struggles with feature extraction, especially in complex backgrounds or with small targets. Transformers [15]–[17] have shown great potential in addressing these limitations. Their self-attention mechanism captures long-range dependencies and global context, making them

effective for small object detection like pulmonary nodules. Incorporating attention mechanisms can thus improve feature representation and reduce both missed detections and false positives.

Inspired by these advancements, we proposed a novel one-stage detection model, **MSDet**, specifically designed to address the challenges of pulmonary nodule detection, including high false positive rates and low detection accuracy. Our contributions include a tiny object detection block (TODB), which captures finer feature details to improve small nodule detection, and an extended receptive domain (ERD) strategy that refines occluded nodule features to reduce false positives. Additionally, we designed the positional channel attention mechanism (PCAM) to optimize feature representation and mitigate high miss and false detection rates in multiscale nodule detection. As shown in Figure 1, **MSDet** achieved a significant **8.8%** improvement in mAP compared to the state-of-the-art nodule detection method YOLOv8.

Hence, this paper proposed three key contributions as follows:

- We proposed **MSDet**, a novel one-stage detection model specifically designed for detecting tiny pulmonary nodules. **MSDet** integrates multiscale attention and an enhanced receptive field, addressing challenges of high false positive rates and low detection accuracy.
- We proposed the extended receptive domain (ERD) strategy to capture richer contextual information and reduce false positives caused by nodule occlusion. We also proposed the position channel attention mechanism (PCAM) to optimize feature learning and reduce multiscale detection errors, and designed the tiny object detection block (TODB) to enhance the detection of tiny nodules.
- We conducted thorough experiments on the public LUNA16 dataset [18], achieving state-of-the-art performance, with an mAP improvement of **8.8%** over the previous state-of-the-art method YOLOv8.

II. RELATED WORKS

Dense prediction techniques [19] have been widely adopted in medical imaging analysis [20]–[23] particularly for tasks such as semantic segmentation [24]–[27], and object detection [28], due to their ability to generate pixel-level predictions that enhance the precision of identifying and localizing anatomical structures or pathological regions. Detection algorithms for pulmonary nodules based on deep learning can be broadly classified into two categories: two-stage detection algorithms and one-stage detection algorithms.

Two-stage detection algorithms, such as R-CNN, first generate candidate regions and then classify and localize targets. Fast R-CNN [5] accelerates detection by sharing convolutional features, while Faster R-CNN [6] improves both speed and accuracy with Region Proposal Networks (RPNs). For instance, Xu et al. [29] enhanced the Faster R-CNN model by adopting multi-scale training strategies, Online Hard Example Mining (OHEM), customized anchor sizes and ratios, deformable convolutions, and path augmentation in Feature

Pyramid Networks (FPNs). This improved model significantly enhanced small target detection capabilities. Su et al. [30] proposed a Faster R-CNN-based method for lung nodule detection, achieving over 20% accuracy improvement compared to traditional algorithms, showing potential clinical value in lung disease diagnosis. Tong et al. [31] proposed a pulmonary nodule detection system using Faster R-CNN with ISODATA [32] for candidate detection and 3D-CNN with Focal Loss for false positive reduction, achieving strong results on LUNA16. However, the primary drawback of two-stage detection algorithms is the time-consuming process of generating candidate regions, which leads to slower detection speeds. Additionally, the generation of candidate regions often relies on prior knowledge, potentially resulting in inaccurate localization, especially when targets vary significantly in shape or size. These limitations hinder the efficiency and performance of two-stage detection algorithms in real-time applications.

One-stage detection algorithms mitigate the limitations of two-stage algorithms by performing object detection directly on the input image without the need for candidate region generation, thus significantly accelerating the detection process. Representative one-stage detection algorithms include the YOLO series and SSD. These algorithms achieve both localization and classification in a single pass, making them highly advantageous in applications requiring real-time performance. In the context of pulmonary nodule detection, the YOLO series has been widely adopted due to its rapid detection speed and high accuracy. For example, Wu et al. [33] proposed a YOLOv7-based method for pulmonary nodule detection that incorporates Efficient Omni-Dimensional Convolution (EOD-Conv) to enhance feature extraction precision, achieving a mAP of 94.6% on the LUNA16 dataset. Additionally, Zhanlin Ji et al. [34] improved the nodule detection performance across different scales by decoupling the feature pyramid into high-semantic and low-semantic regions to reduce semantic conflicts during fusion, achieving an accuracy of 92.3% on the Lung-PETCT-Dx dataset.

However, one-stage detection algorithms face challenges due to multiple down-sampling steps, which progressively reduce the feature map size. This reduction causes the size of small pulmonary nodules on the feature map to become very small, potentially leading to the loss of fine features and making small nodules difficult to detect. Moreover, in the complex pulmonary environment, lung tissues often occlude nodules, further complicating accurate detection. These challenges result in missed detections, false positives, and high false-positive rates for occluded nodules. To address these issues, this paper proposes a novel one-stage detection network designed to integrate multiple modules specifically aimed at efficiently and accurately detecting small pulmonary nodules. This network achieves precise detection of small nodules and accurate and efficient detection of occluded and multi-scale nodules within complex pulmonary environments.

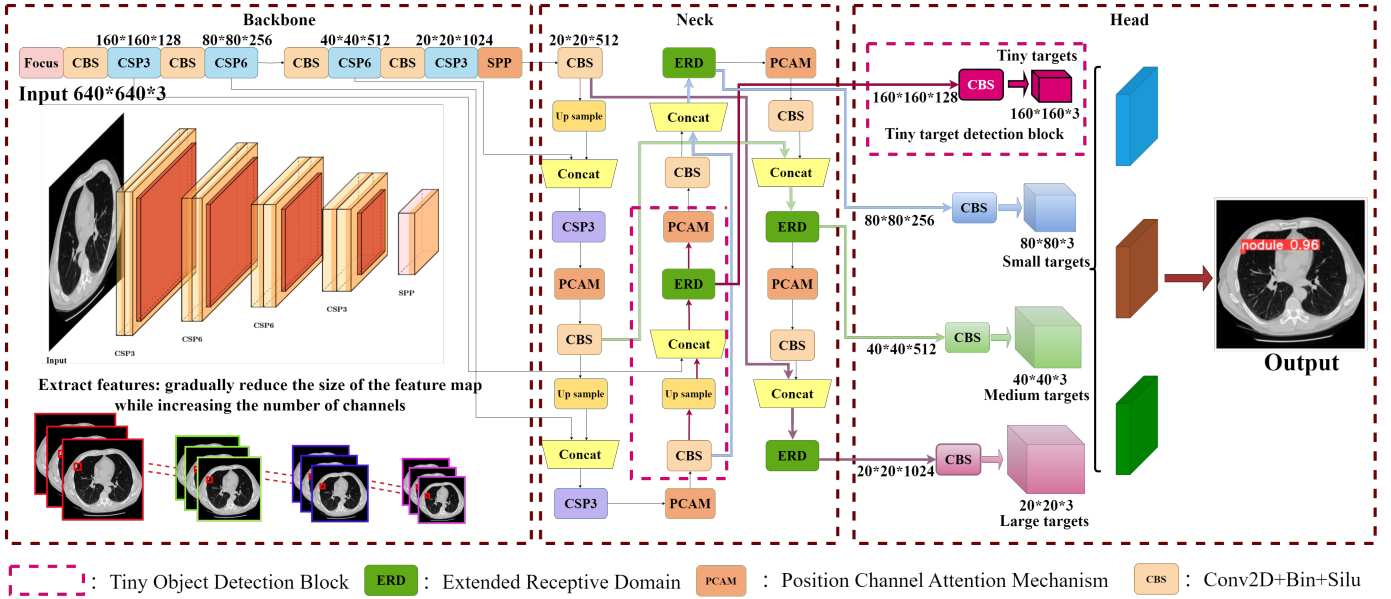


Fig. 2. Overall architecture of the MSDet network for lung nodule detection. The initial convolutional layers, represented as CBS blocks, process the input lung CT image to extract preliminary features. These features undergo a series of transformations through the ERD modules, which broaden the receptive field to capture more contextual information. PCAM modules are strategically placed to refine feature representation by focusing on crucial spatial and channel-related information. Multiple feature maps generated at different stages are then concatenated and further processed through upsampling and additional CBS blocks to construct refined prediction feature maps.

III. METHODS

A. Overview

We proposed a novel lung nodule detection network MSDet. The overall architecture of MSDet is shown in Figure 2. Our method captures richer contextual information and reduces false positives caused by nodule occlusion through the extended receptive domain (ERD) strategy. Then, we design a dedicated position channel attention mechanism (PCAM) to effectively optimize feature learning and reduce multi-scale detection errors. Finally, the connection between different feature maps is captured by the design of the tiny object detection block (TODB), which reduces the interference of complex background tissues and aims to improve the detection accuracy of small nodules of the model. Specifically, given a lung CT image input, after convolution and feature fusion operations, multi-scale feature fusion and information transfer are realized. In the feature fusion stage, the feature map size is restored by the TODB through upsampling operation, and it is fused with feature maps of different resolutions to generate a more refined prediction feature map. Then, following the concatenation operation, the multiscale feature maps are connected and input into the ERD module designed by us, which effectively expands the receptive field of the feature map, captures more contextual information and details, and enables the network to integrate information from a larger area. As shown in Figure 3, the SPP module further enhances this capability by aggregating features at multiple scales, improving the robustness of the feature representation against variations in object size and position. A key aspect of our design is the PCAM. In the PCAM module, the position

attention module captures long-range contextual information, while the channel attention module models the interdependencies between channels, thereby adjusting the attention weights according to the importance of different positions and channels. Finally, the model generates output feature maps at multiple scales to produce the final prediction results.

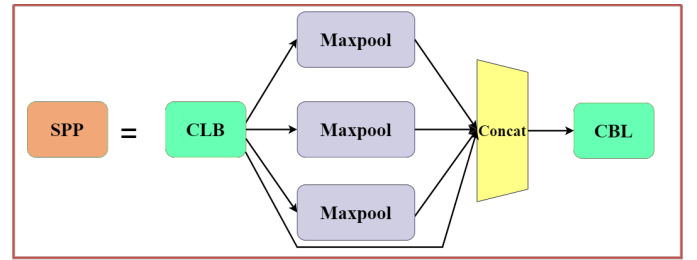


Fig. 3. Architecture of the Spatial Pyramid Pooling (SPP) module. The module utilizes a Convolutional Layer Block (CLB) followed by three parallel Maxpool layers with varying sizes to capture multi-scale features. These features are then concatenated and processed by another CLB to enhance the final feature representation, ensuring robust spatial invariance.

B. Tiny Object Detection Block (TODB)

The vanilla YOLOv5, primarily designed for handling natural images, shows limited efficacy in detecting pulmonary nodules in CT images. During network downsampling, the deepest feature map size is reduced to 20×20 pixels. In the YOLOv5, multiple downsampling operations progressively reduce the feature map size, causing small pulmonary nodules to appear extremely tiny in the feature maps. For example, a $32 \times$ downsampling reduces a 20×20 pixel nodule to 1×1 pixel,

making it nearly undetectable. As a result, YOLOv5 performs poorly on pulmonary nodule detection in CT scans.

To address this challenge, we designed the TODB module to capture the relationships between different feature maps. This module aims to minimize interference from complex surrounding tissues in medical images, thereby enhancing the recognition accuracy of small nodules. By leveraging the TODB module, the network can more effectively extract and identify features of pulmonary nodules, improving detection accuracy. Figure 4 illustrates the specific structure of the TODB, which optimizes feature map connections and information extraction, significantly boosting the detection performance of small nodules as detailed below.

The network input size is $640 \times 640 \times 3$, and after a series of downsampling operations, an $80 \times 80 \times 128$ feature map F_1 is generated. To enrich it with contextual information, a 1×1 convolution is applied, altering the channel number for cross-channel interaction, enhancing nodule detection. This operation is expressed as:

$$F'_1 = \sigma(W_1 * F_1) \quad (1)$$

where σ is the activation function and $*$ denotes convolution. Next, F_1 is upsampled to $160 \times 160 \times 64$ and added to another feature map F_2 , obtained via a 4x downsampling of the input. This operation combines multi-resolution features to improve detection accuracy, expressed as:

$$F_3 = \text{Upsample}(F'_1) + F_2 \quad (2)$$

After further convolutional processing, the final output F_4 is generated, which is a $160 \times 160 \times 18$ feature map used for nodule prediction:

$$F_4 = \sigma(W_2 * F_3) \quad (3)$$

This process divides the input into 160×160 regions for precise nodule prediction, efficiently integrating multi-resolution and cross-channel information to enhance detection accuracy. By concentrating on smaller regions and leveraging multi-scale features, the model's robustness is greatly enhanced.

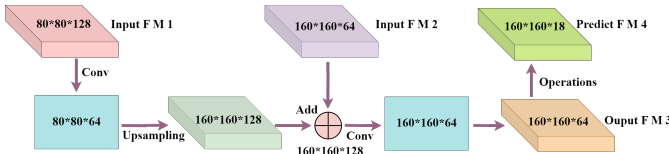


Fig. 4. TODB Structure. This module integrates multi-resolution features through upsampling and feature map fusion, allowing the network to capture small pulmonary nodules more accurately. The structure enhances detection robustness by combining features from different resolutions.

C. Extended Receptive Domain (ERD)

Decoupling the network's bottleneck structures can enhance lung nodule detection but may reduce the receptive field, limiting the ability to capture global contextual information. To address this, we propose an extended receptive domain (ERD)

strategy, which expands the receptive field while maintaining computational efficiency, allowing for improved detection of nodules across various sizes and scales.

As shown in Figure 6, ERD uses a multi-branch structure to capture multiscale features. It integrates three parallel 3×3 dilated convolution branches, a 1×1 convolution branch, and an identity branch. The dilated convolutions use dilation rates $R = (1, 3, 5)$ to provide varying receptive fields while keeping the resolution intact by setting the padding to $P = (1, 3, 5)$. The 1×1 convolution branch captures fine details and enhances positional information.

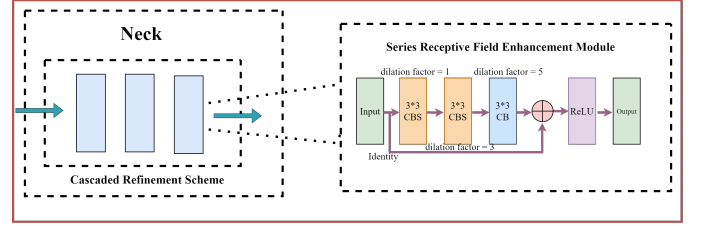


Fig. 5. Illustration of the ERD architecture integrating multiple dilated convolutions for lung nodule detection. The diagram on the left shows the Neck with a Cascaded Refinement Scheme, and the right side details the Series Receptive Field Enhancement Module, employing dilated convolutions with varying dilation factors to capture multiscale features effectively.

Dilated convolutions introduce fixed gaps between kernel values, allowing expansion of the receptive field without increasing the number of parameters. The output of a dilated convolution with input $x(m, n)$ and kernel weights $\omega(i, j)$ can be expressed as:

$$y(m, n) = \sum_{i=1}^M \sum_{j=1}^N x(m + r \cdot i + n + r \cdot j) \omega(i, j) \quad (4)$$

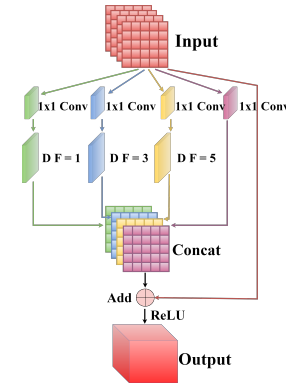


Fig. 6. ERD Structure. The ERD consists of multiple parallel convolution branches with varying dilation rates, designed to capture features at different spatial scales. This structure enhances the detection of lung nodules by expanding the receptive field while maintaining computational efficiency.

where r is the dilation rate, and M, N are kernel sizes (typically 3×3). By varying r , the receptive field expands: $r = 1$ results in a 3×3 receptive field, $r = 2$ gives 5×5 , and $r = 3$ gives 7×7 , all while keeping the computation similar to a standard convolution.

As illustrated in Figure 5, the ERD strategy employs a sophisticated multi-branch structure to effectively capture features at multiple scales. This figure visually demonstrates the arrangement and interaction of various convolution branches within the ERD, highlighting the specific roles of dilated and 1×1 convolutions in enhancing the model's sensitivity to spatial details and contextual variations across different nodule sizes.

The equivalent receptive field (RF) for a $k \times k$ dilated convolution and the output feature map resolution (H) are calculated as:

$$\text{RF} = (r - 1)(k - 1) + k \quad (5)$$

$$H = \frac{(h + 2p - \text{RF})}{s} + 1 \quad (6)$$

where p is the padding, h is the input feature map resolution, and s is the stride. This method enables efficient scaling of the receptive field without increasing computational cost or altering the spatial resolution of the feature maps.

D. Position Channel Attention Mechanism (PCAM)

Attention mechanisms in CNNs highlight key image features while suppressing irrelevant information, improving model performance. Existing methods primarily rely on first-order statistics, limiting their ability to capture complex feature interactions. To address this, we propose PCAM, as shown in Figure 7, which incorporates higher-order statistics to improve the representation of complex activation features, and is applied to the bottleneck of the MSDet model to enhance focus on key regions in pulmonary nodule images.

PCAM consists of a positional attention module and a channel attention module. The positional attention module captures long-range spatial dependencies by encoding contextual information into local features. Given a feature map $Q \in \mathbb{R}^{C \times H \times W}$, we generate two feature maps, R and S , and compute a spatial attention map $U \in \mathbb{R}^{N \times N}$ as follows:

$$u_{ji} = \frac{e^{(R_i \cdot S_j)}}{\sum_{i=1}^N e^{(R_i \cdot S_j)}} \quad (7)$$

Here, u_{ji} represents the correlation between positions i and j . The resulting attention-weighted feature map is then added to the original features, scaled by a learned parameter β :

$$V_j = \beta \sum_{i=1}^N (u_{ji} T_i) + Q_j \quad (8)$$

Similarly, the channel attention module models dependencies between feature channels. Given Q , the channel attention map $Z \in \mathbb{R}^{C \times C}$ is computed as:

$$z_{ji} = \frac{e^{(Q_i \cdot Q_j)}}{\sum_{i=1}^C e^{(Q_i \cdot Q_j)}} \quad (9)$$

The final feature map is computed as:

$$V_j = \gamma \sum_{i=1}^C (z_{ji} Q_i) + Q_j \quad (10)$$

Both β and γ are initialized to 0 and learn appropriate weights during training. By combining positional and channel attention, PCAM effectively enhances feature discriminability.

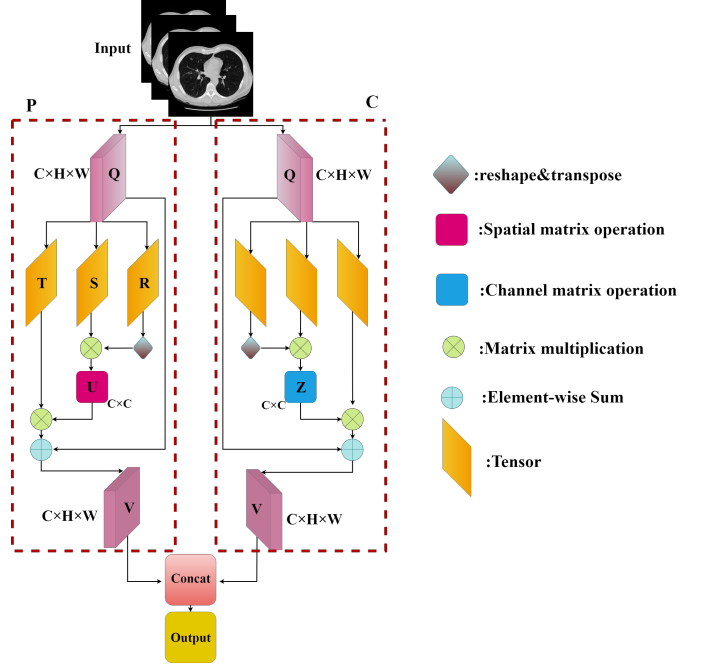


Fig. 7. PCAM Structure. The diagram illustrates the PCAM employing a dual-module approach to capture and integrate complex feature interactions through spatial and channel attentions. This innovative mechanism leverages higher-order statistics to enhance activation feature characterization, optimizing the performance for intricate image analysis challenges.

IV. EXPERIMENTS

A. Dataset and Evaluation Matrices

The experimental data utilized in this study were obtained from the publicly available LUNA16 lung CT imaging dataset. The LUNA16 dataset is derived from the LIDC-IDRI dataset, with slices thicker than 3 mm and nodules smaller than 3 mm removed, encompassing a total of 888 cases. To facilitate analysis, we converted the three-dimensional data into two-dimensional slices.

In terms of evaluation metrics, the performance of the pulmonary nodule detection model is assessed using several standard measures. Precision quantifies the accuracy of positively predicted instances, aiming to minimize false positives. Recall evaluates the model's ability to identify all relevant cases [35], which is crucial for thorough detection. The F1-score merges precision and recall in a single metric, reflecting the balance between detection accuracy and completeness. Average Precision (AP), calculated over the Precision-Recall curve, provides detailed insights into the model's precision across various recall levels. Mean Average Precision (mAP)

averages these AP values across different object classes and sizes, offering a global view of the model’s overall accuracy.

B. Implementation Details

The proposed MSDet model was implemented using the PyTorch 1.13.1 framework and trained on an NVIDIA GPU. The batch size was set to 8, and training spanned 200 epochs. We employed the SGD optimizer with a momentum of 0.937 and an initial learning rate of 0.01. Data augmentation techniques, including random rotations, flips, brightness, contrast, and color adjustments, along with salt-and-pepper noise, were applied to enhance model robustness.

Prior to training, the data underwent a comprehensive pre-processing phase. The CT image grayscale values were first converted to Hounsfield Units (HU), which reflect the radiodensity of human tissues, with lung tissue typically around -500 HU. During preprocessing, we retained regions with HU values between -1000 and 400 while truncating values outside this range. The raw data were then clipped to a range of [-1200, 600], setting values below -1200 and above 600 to -1200 and 600 respectively, effectively filtering out elements like water and air. Lung parenchyma segmentation was performed using erosion to remove granular regions, followed by dilation to encompass blood vessels and eliminate black noise from non-transparent rays within the lung regions. The central part of the CT image was selected for lung mask extraction, focusing on the largest connected component, which was further dilated to fully capture the lung region. If the edges remained uneven, additional erosion was applied to refine them. Finally, the preprocessed images were normalized to a range of 0 to 255, completing the data preprocessing pipeline.

After preprocessing, the performance of the models was evaluated using standard metrics such as $mAP_{0.5}$ and mAP at 0.5 to 0.95. MSDet consistently outperformed models like YOLOv3, YOLOv7, Scaled_YOLOv4, and TPH-YOLOv5, achieving a 60% mAP at 0.5 to 0.95 after 125 epochs, demonstrating higher precision and recall with fewer training iterations.

The lung nodule detection workflow is depicted in Figure 8.

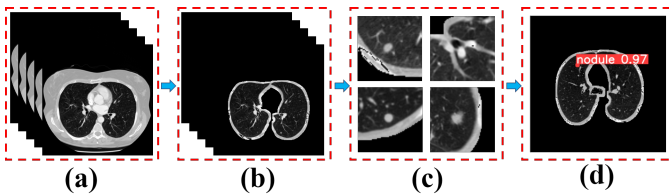


Fig. 8. Illustration of the pulmonary nodule detection process using the MSDet model. The sequence shows (a) the initial input CT image, (b) processed two-dimensional slices after image preprocessing, (c) zoomed-in views highlighting candidate nodules after candidate detection, and (d) the final detection results with a confidence score.

C. Comparative Studies

We conducted comparative analyses using the LUNA16 lung nodule detection dataset with state-of-the-art methods, as

shown in Table III. The results demonstrate that our proposed MSDet algorithm significantly outperforms various leading lung nodule detection models.

Specifically, MSDet achieved a mAP of 97.3%, surpassing several popular models. Notably, MSDet exceeded the performance of the two-stage model Faster R-CNN by 6.6 percentage points and outperformed the DLDS-CT method by 16.1 percentage points. Furthermore, compared to recent YOLO models, MSDet demonstrated improvements of 11.5%, 14.51%, 16.02%, and 8.8% over YOLOv5, YOLOv6, YOLOv7, and YOLOv8, respectively.

In addition, MSDet outperformed EfficientDet-d, CenterNet, YOLOv5-CASP, and YOLO-MSRF models, with mAP improvements of 9.9%, 12%, 25.3%, and 2.7%, respectively. These results indicate the overall superiority of MSDet in terms of detection accuracy and efficiency. The experimental findings validate the robustness and effectiveness of our proposed approach in lung nodule detection.

D. Ablation Studies

The ablation study results in Table I demonstrate that both TODB and ERD significantly improve the performance of the Basic Model on the LUNA16 dataset. TODB alone increased precision from 83.7% to 88.4%, recall from 81.3% to 87.2%, and $mAP_{0.5}$ from 84.7% to 89.1%. Similarly, ERD alone improved precision to 88.5%, recall to 87.6%, and $mAP_{0.5}$ to 88.9%. When combined with other modules (ERD, TODB, and PCAM), these metrics reached their highest values: 97.2% precision, 96.1% recall, and 97.3% $mAP_{0.5}$. These results highlight the significant role of TODB and ERD in enhancing detection precision, recall, and overall performance in lung nodule detection.

As shown in Table II and Table I, the PCAM (Ours) module further enhances pulmonary nodule detection. With a precision of 93.1%, recall of 92.5%, and an F1 score of 92.8%, PCAM effectively balances precision and recall while minimizing false positives. It also achieves superior mAP scores across various IoU thresholds, demonstrating robust detection performance for nodules of different sizes. The integration of position-sensitive and channel attention mechanisms enhances multi-scale detection, as illustrated in Figure 9. The ablation study confirms PCAM’s impact on the Basic Model’s performance on the LUNA16 dataset. With PCAM alone, precision increased from 83.7% to 87.1%, recall from 81.3% to 88.7%, and $mAP_{0.5}$ from 84.7% to 88.3%. When combined with TODB and ERD, these metrics reached final values of 97.2% precision, 96.1% recall, and 97.3% $mAP_{0.5}$, underscoring PCAM’s effectiveness in boosting detection accuracy and overall performance.

E. Discussion

1) *Clinical Impact*: MSDet’s multiscale detection and attention mechanisms, including ERD and PCAM, address key challenges in identifying small and occluded pulmonary nodules, which are often missed due to their size and complex surroundings. By enhancing detection accuracy and reducing

TABLE I

ABLATION STUDY OF MSDet ON THE LUNA16 DATASET, EVALUATING THE IMPACT OF DIFFERENT MODULES (TODB, ERD, AND PCAM) ON DETECTION PERFORMANCE. THE TABLE PRESENTS THE PRECISION, RECALL, AND $mAP_{0.5}$ RESULTS FOR VARIOUS CONFIGURATIONS OF THE MSDet MODEL, DEMONSTRATING SIGNIFICANT IMPROVEMENTS WHEN ALL MODULES ARE COMBINED.

YOLOv5	TODB	ERD	PCAM	Precision (%)	Recall (%)	$mAP_{0.5}$ (%)
✓				83.7 ± 0.09	81.3 ± 0.07	84.7 ± 0.03
✓	✓			88.4 ± 0.04	87.2 ± 0.05	89.1 ± 0.08
✓		✓		88.5 ± 0.02	87.6 ± 0.06	88.9 ± 0.04
✓			✓	87.1 ± 0.09	88.7 ± 0.05	88.3 ± 0.07
✓	✓	✓		91.6 ± 0.08	90.1 ± 0.06	92.8 ± 0.02
✓	✓		✓	91.4 ± 0.04	91.2 ± 0.03	92.5 ± 0.08
✓		✓	✓	91.2 ± 0.09	91.4 ± 0.05	91.9 ± 0.01
✓	✓	✓	✓	97.2 ± 0.06	96.1 ± 0.05	97.3 ± 0.03

TABLE II

DETECTION PERFORMANCE COMPARISON USING DIFFERENT ATTENTION MODULES ON THE LUNA16 DATASET. THIS TABLE PRESENTS PRECISION, RECALL, F1 SCORE, AND MAP RESULTS ACROSS VARIOUS IOU THRESHOLDS AND NODULE SIZES, DEMONSTRATING THE SUPERIOR PERFORMANCE OF THE PCAM (OURS) MODULE COMPARED TO OTHER STATE-OF-THE-ART ATTENTION MECHANISMS.

Methods	Precision(%)	Recall(%)	F1Score(%)	$mAP_{0.5}$ (%)	$mAP_{0.75}$ (%)	$mAP_{0.95}$ (%)	mAP_S (%)	mAP_M (%)	mAP_L (%)
SE [36]	89.5 ± 0.02	90.1 ± 0.04	89.8 ± 0.06	89.7 ± 0.03	79.2 ± 0.08	60.7 ± 0.09	67.4 ± 0.1	74.1 ± 0.02	80.1 ± 0.08
CBAM [37]	91.4 ± 0.1	91.9 ± 0.03	91.6 ± 0.08	91.7 ± 0.03	81.1 ± 0.1	63.2 ± 0.04	68.1 ± 0.07	75.2 ± 0.05	81.4 ± 0.02
SA [38]	89.8 ± 0.06	90.6 ± 0.07	90.2 ± 0.01	90.2 ± 0.09	79.8 ± 0.08	61.1 ± 0.03	67.1 ± 0.03	74.0 ± 0.06	80.5 ± 0.01
NAM [39]	88.6 ± 0.1	89.1 ± 0.06	88.8 ± 0.03	88.4 ± 0.02	79.1 ± 0.08	60.4 ± 0.08	67.3 ± 0.09	74.7 ± 0.04	80.3 ± 0.07
CA [40]	90.3 ± 0.04	89.7 ± 0.07	89.9 ± 0.08	90.1 ± 0.09	79.4 ± 0.03	61.6 ± 0.04	67.6 ± 0.02	75.1 ± 0.05	81.0 ± 0.09
ECA [41]	89.5 ± 0.09	90.2 ± 0.06	89.8 ± 0.06	89.7 ± 0.03	79.6 ± 0.07	60.8 ± 0.02	67.9 ± 0.08	74.1 ± 0.1	80.2 ± 0.1
NLNN [42]	90.4 ± 0.1	90.6 ± 0.03	89.6 ± 0.05	89.2 ± 0.02	79.4 ± 0.07	61.2 ± 0.09	67.2 ± 0.05	74.9 ± 0.04	81.1 ± 0.08
GAT [43]	89.2 ± 0.03	89.7 ± 0.01	89.4 ± 0.05	89.8 ± 0.09	80.5 ± 0.1	60.7 ± 0.07	67.0 ± 0.04	74.6 ± 0.02	80.7 ± 0.08
BAM [44]	89.8 ± 0.07	90.2 ± 0.08	90.2 ± 0.07	90.5 ± 0.04	80.1 ± 0.02	61.4 ± 0.06	67.9 ± 0.1	74.8 ± 0.05	81.0 ± 0.01
MAB [15]	90.9 ± 0.02	91.2 ± 0.05	91.1 ± 0.03	91.3 ± 0.06	79.9 ± 0.09	61.9 ± 0.08	68.1 ± 0.02	75.1 ± 0.03	80.2 ± 0.1
CCA [45]	91.4 ± 0.1	91.8 ± 0.07	91.6 ± 0.02	91.5 ± 0.09	80.2 ± 0.01	62.3 ± 0.03	68.0 ± 0.05	74.4 ± 0.04	80.4 ± 0.06
SOCA [46]	90.7 ± 0.07	90.3 ± 0.06	90.5 ± 0.02	90.3 ± 0.1	80.6 ± 0.03	61.7 ± 0.1	68.2 ± 0.04	75.0 ± 0.08	81.5 ± 0.04
PCAM (Ours)	93.1 ± 0.05	92.5 ± 0.04	92.8 ± 0.07	93.7 ± 0.05	83.7 ± 0.1	65.8 ± 0.03	70.6 ± 0.03	77.1 ± 0.06	83.7 ± 0.07

TABLE III

COMPARISON OF MSDet WITH STATE-OF-THE-ART LUNG NODULE DETECTION NETWORKS IN TERMS OF MAP. THE TABLE HIGHLIGHTS THE SUPERIOR PERFORMANCE OF MSDet COMPARED TO WIDELY-USED MODELS SUCH AS YOLO, FASTER R-CNN, AND LUNGSEEK, DEMONSTRATING THE ROBUSTNESS OF OUR APPROACH IN ACHIEVING HIGHER DETECTION ACCURACY.

Model	mAP
YOLOv5 [47]	85.8%
YOLOv6 [48]	82.79%
YOLOv7 [49]	81.28%
YOLOv8 [50]	88.5%
Faster R-CNN [29]	90.7%
Two-Stage CNN [51]	84.4%
LungSeek [52]	91.75%
DLDS-CT [53]	81.2%
EfficientDet-d [54]	87.4%
CenterNet [55]	85.3%
STBi-YOLO [56]	95.9%
YOLOv5-CASP [57]	72.0%
YOLO-MSRF [33]	94.6%
MSDet (Ours)	97.3%

false positives, MSDet assists radiologists in early malignancy identification, boosting diagnostic confidence and enabling timely interventions. Its integration into clinical workflows can streamline lung cancer screening by automating nodule detection, reducing the radiologists' workload, and allowing them to focus on critical cases. MSDet's lightweight architecture supports real-time deployment without compromising speed or accuracy, making it well-suited for high-volume imaging environments. As screening programs expand, MSDet can help prioritize urgent cases and ease the burden on healthcare systems.

2) *Contributions to Early Diagnosis and Broader Societal Impact:* MSDet's precise detection of small pulmonary nodules facilitates earlier lung cancer diagnoses, improving survival rates and enabling less invasive treatments. By reducing false positives, it minimizes unnecessary follow-ups, alleviating patient stress and lowering healthcare costs. This enhanced accuracy streamlines the diagnostic process, making healthcare more efficient. Globally, MSDet can have a transformative impact, especially in regions with limited access to radiologists. By providing high-quality automated screening, it helps bridge healthcare disparities, ensuring timely and accurate diagnoses for all patients. Ultimately, MSDet contributes to improved patient outcomes, reduced lung cancer mortality, and lower healthcare burdens.

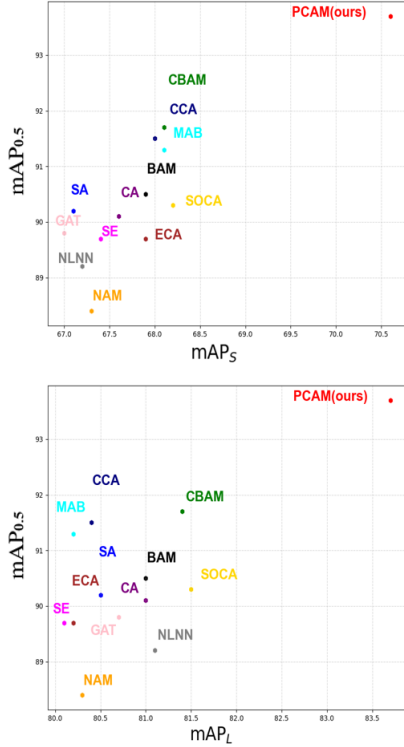


Fig. 9. Comparison chart of $mAP_S - mAP_L - mAP_{0.5}$. The y-axis corresponds to $mAP_{0.5}$ (mean Average Precision at IoU threshold of 0.5), where higher values indicate better performance. The x-axis represents the detection performance of micro-small and relatively large pulmonary nodules. Our method, PCAM, achieved the best balance between performance and accuracy in multi-scale pulmonary nodule detection.

F. Visualization

In this section, we present a visual comparison of the detection results to validate the effectiveness of the proposed MSDet model for lung nodule detection. As illustrated in Figure 10, MSDet consistently outperforms YOLOv4, Scaled_YOLOv4, and the Basic Model across various scenarios, including both single and multiple nodule detections. For instance, MSDet achieved 94% accuracy in detecting nodules in complex imaging backgrounds, while YOLOv4 and Scaled_YOLOv4 exhibited lower accuracies due to false positives and false negatives. In multi-nodule cases, MSDet demonstrated superior precision, accurately identifying all nodules without false positives or false negatives, outperforming the other models by 6% to 8%. These results emphasize the robustness and accuracy of MSDet, especially in handling complex imaging conditions and challenging nodules, making it highly reliable for clinical applications.

Lung parenchyma segmentation further enhances detection accuracy by providing cleaner image backgrounds. This process involves renormalizing the images, using K-means clustering to separate lung tissue from the background, and refining the lung mask through erosion and dilation. As shown in Figure 11, models such as YOLOv4, Scaled_YOLOv4, the

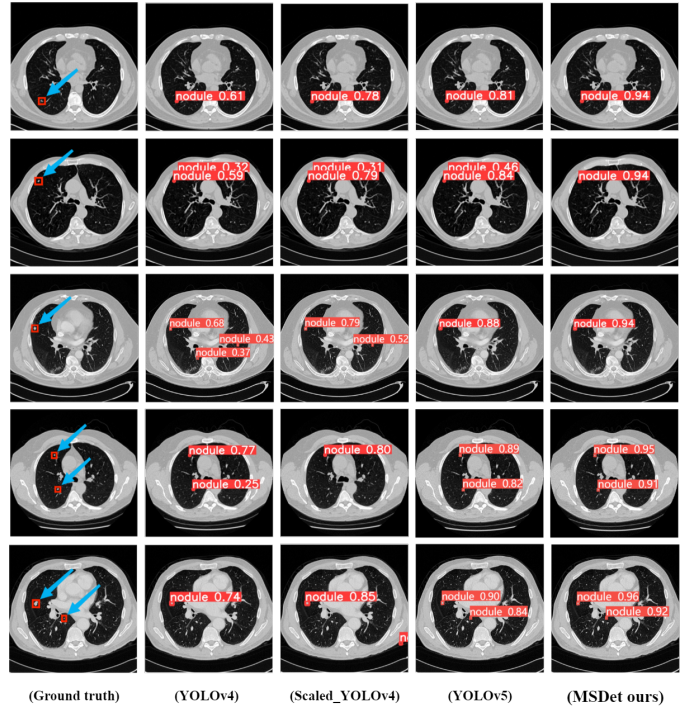


Fig. 10. Visual comparison of lung nodule detection results on the LUNA16 dataset, highlighting MSDet’s superior performance compared with other models. The figure illustrates MSDet’s effectiveness in reducing false positives and achieving higher accuracy, showcasing its robustness for clinical applications.

Basic Model, and MSDet demonstrate improved performance post-segmentation compared to raw data. MSDet, in particular, achieved up to 98% accuracy in detecting multiple nodules, reducing both false positives and false negatives. Overall, lung parenchyma segmentation significantly boosts detection precision across all models, highlighting its importance in complex imaging tasks.

V. CONCLUSION

This paper proposes a novel method, MSDet, for lung nodule detection in CT images, specifically designed to address multi-scale nodule detection and ensure accurate identification. To overcome the limitations of traditional algorithms in detecting small nodules, we introduced TODB, which enhances feature extraction for tiny lung nodules. Additionally, we designed an ERD strategy to refine occluded nodule features by constructing an effective receptive field, enabling accurate detection of occluded nodules. Furthermore, we proposed a new attention mechanism, PCAM, which adjusts attention weights based on the importance of different positions and channels. This optimizes feature representation learning and improves adaptability to nodules of varying scales, thereby reducing missed and false detections. In summary, MSDet presents a novel framework for multi-scale tiny nodule detection. Empirical validation demonstrates that our model not only detects small nodules effectively in complex backgrounds but also surpasses existing benchmarks on the public LUNA16

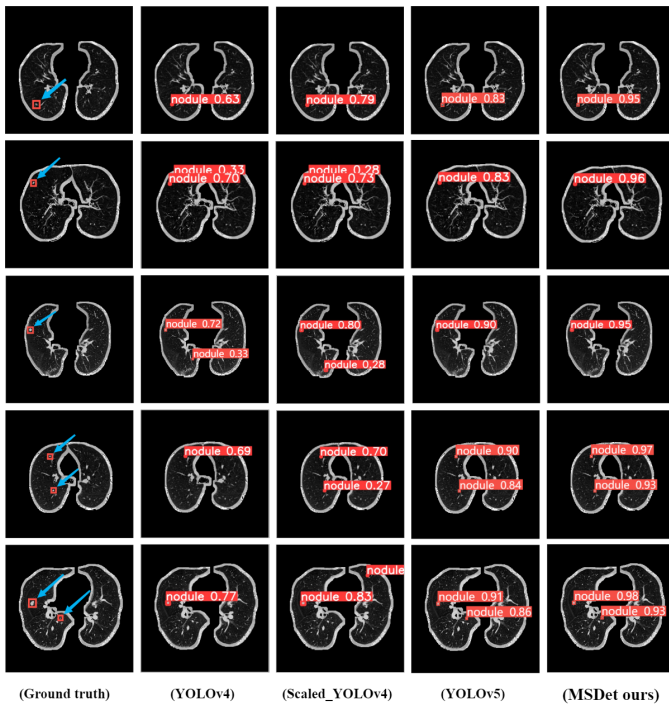


Fig. 11. Visual comparison of lung nodule detection results on the LUNA16 dataset, illustrating the impact of lung parenchyma segmentation on improving detection accuracy. MSDet shows a notable reduction in false positives and an accuracy of up to 98% in complex scenarios, highlighting the effectiveness of segmentation in enhancing the clarity and precision of nodule detection across different algorithms.

dataset. This study marks a significant advancement in medical image detection, with the potential to profoundly influence future medical image processing endeavors.

ACKNOWLEDGMENT

This work was supported by the National Natural Science Foundation of China (Grant No. 62306027) and Southwest Minzu University. We would like to express our gratitude to our collaborators for their valuable contributions and support throughout this study.

REFERENCES

- [1] R. L. Siegel, A. N. Giaquinto, A. Jemal, Cancer statistics, 2024, CA: a cancer journal for clinicians 74 (1) (2024) 12–49.
- [2] E. R. Núñez, S. Zhang, M. E. Glickman, S. X. Qian, J. H. Boudreau, P. K. Lindenauer, C. G. Slatore, D. R. Miller, T. J. Caverly, R. S. Wiener, What goes into patient selection for lung cancer screening? factors associated with clinician judgments of suitability for screening, American journal of respiratory and critical care medicine 209 (2) (2024) 197–205.
- [3] T. L. Leong, A. McWilliams, G. M. Wright, Incidental pulmonary nodules: An opportunity to complement lung cancer screening, Journal of Thoracic Oncology 19 (4) (2024) 522–524.
- [4] R. Girshick, J. Donahue, T. Darrell, J. Malik, Rich feature hierarchies for accurate object detection and semantic segmentation, in: Proceedings of the IEEE conference on computer vision and pattern recognition, 2014, pp. 580–587.
- [5] R. Girshick, Fast r-cnn, in: Proceedings of the IEEE international conference on computer vision, 2015, pp. 1440–1448.
- [6] S. Ren, K. He, R. Girshick, J. Sun, Faster r-cnn: Towards real-time object detection with region proposal networks, IEEE transactions on pattern analysis and machine intelligence 39 (6) (2016) 1137–1149.

- [7] K. He, G. Gkioxari, P. Dollár, R. Girshick, Mask r-cnn, in: Proceedings of the IEEE international conference on computer vision, 2017, pp. 2961–2969.
- [8] J. Redmon, S. Divvala, R. Girshick, A. Farhadi, You only look once: Unified, real-time object detection, in: Proceedings of the IEEE conference on computer vision and pattern recognition, 2016, pp. 779–788.
- [9] J. Redmon, A. Farhadi, Yolo9000: better, faster, stronger, in: Proceedings of the IEEE conference on computer vision and pattern recognition, 2017, pp. 7263–7271.
- [10] J. Redmon, A. Farhadi, Yolov3: An incremental improvement, arXiv preprint arXiv:1804.02767 (2018).
- [11] A. Bochkovskiy, C.-Y. Wang, H.-Y. M. Liao, Yolov4: Optimal speed and accuracy of object detection, arXiv preprint arXiv:2004.10934 (2020).
- [12] W. Liu, D. Anguelov, D. Erhan, C. Szegedy, S. Reed, C.-Y. Fu, A. C. Berg, Ssd: Single shot multibox detector, in: Computer Vision—ECCV 2016: 14th European Conference, Amsterdam, The Netherlands, October 11–14, 2016, Proceedings, Part I 14, Springer, 2016, pp. 21–37.
- [13] K. Duan, S. Bai, L. Xie, H. Qi, Q. Huang, Q. Tian, Centernet: Keypoint triplets for object detection, in: Proceedings of the IEEE/CVF international conference on computer vision, 2019, pp. 6569–6578.
- [14] T.-Y. Lin, P. Goyal, R. Girshick, K. He, P. Dollár, Focal loss for dense object detection, in: Proceedings of the IEEE international conference on computer vision, 2017, pp. 2980–2988.
- [15] A. Vaswani, N. Shazeer, N. Parmar, J. Uszkoreit, L. Jones, A. N. Gomez, Ł. Kaiser, I. Polosukhin, Attention is all you need, Advances in neural information processing systems 30 (2017).
- [16] A. Dosovitskiy, L. Beyer, A. Kolesnikov, D. Weissenborn, X. Zhai, T. Unterthiner, M. Dehghani, M. Minderer, G. Heigold, S. Gelly, et al., An image is worth 16x16 words: Transformers for image recognition at scale, in: International Conference on Learning Representations, 2020.
- [17] Y. Ji, H. Saratchandran, C. Gordon, Z. Zhang, S. Lucey, Sine activated low-rank matrices for parameter efficient learning, arXiv preprint arXiv:2403.19243 (2024).
- [18] A. A. Setio, A. Traverso, T. De Bel, M. S. Berens, C. Van Den Bogaard, P. Cerello, H. Chen, Q. Dou, M. E. Fantacci, B. Geurts, et al., Validation, comparison, and combination of algorithms for automatic detection of pulmonary nodules in computed tomography images: the luna16 challenge, Medical image analysis 42 (2017) 1–13.
- [19] J. Ge, Z. Zhang, M. H. Phan, B. Zhang, A. Liu, Y. Zhao, Esa: Annotation-efficient active learning for semantic segmentation, arXiv preprint arXiv:2408.13491 (2024).
- [20] B. Wu, Y. Xie, Z. Zhang, M. H. Phan, Q. Chen, L. Chen, Q. Wu, Xlip: Cross-modal attention masked modelling for medical language-image pre-training, arXiv preprint arXiv:2407.19546 (2024).
- [21] Y. Zhao, Z. Liao, Y. Liu, K. O. Nijhuis, B. Barvelink, J. Puijts, J. Colaris, M. Wijffels, M. Reijman, Z. Zhang, et al., A landmark-based approach for instability prediction in distal radius fractures, in: 2024 IEEE International Symposium on Biomedical Imaging (ISBI), IEEE, 2024, pp. 1–5.
- [22] A. D. Hiwase, C. D. Oviden, L. M. Kaukas, M. Finnis, Z. Zhang, S. O'Connor, N. Foo, B. Reddi, A. J. Wells, D. Y. Ellis, Can rotational thromboelastometry rapidly identify therapeutic targets in isolated traumatic brain injury?, Emergency Medicine Australasia (2024).
- [23] Z. Zhang, X. Qi, M. Chen, G. Li, R. Pham, A. Qassim, E. Berry, Z. Liao, O. Siggs, R. Mclaughlin, et al., Jointvit: Modeling oxygen saturation levels with joint supervision on long-tailed octa, in: Annual Conference on Medical Image Understanding and Analysis, Springer, 2024, pp. 158–172.
- [24] B. Wu, Y. Xie, Z. Zhang, J. Ge, K. Yaxley, S. Bahadir, Q. Wu, Y. Liu, M.-S. To, Bhsd: A 3d multi-class brain hemorrhage segmentation dataset, in: International Workshop on Machine Learning in Medical Imaging, Springer, 2023, pp. 147–156.
- [25] Z. Zhang, X. Qi, B. Zhang, B. Wu, H. Le, B. Jeong, Z. Liao, Y. Liu, J. Verjans, M.-S. To, et al., Segreg: Segmenting oars by registering mr images and ct annotations, in: 2024 IEEE International Symposium on Biomedical Imaging (ISBI), IEEE, 2024, pp. 1–5.
- [26] S. Tan, Z. Zhang, Y. Cai, D. Ergu, L. Wu, B. Hu, P. Yu, Y. Zhao, Segstitch: Multidimensional transformer for robust and efficient medical imaging segmentation, arXiv preprint arXiv:2408.00496 (2024).
- [27] Z. Zhang, B. Zhang, A. Hiwase, C. Barras, F. Chen, B. Wu, A. J. Wells, D. Y. Ellis, B. Reddi, A. W. Burgan, M.-S. To, I. Reid, R. Hartley, Thin-thick adapter: Segmenting thin scans using thick annotations, OpenReview (2023).

- [28] Z. Zhang, N. Yi, S. Tan, Y. Cai, Y. Yang, L. Xu, Q. Li, Z. Yi, D. Ergu, Y. Zhao, Meddet: Generative adversarial distillation for efficient cervical disc herniation detection, arXiv preprint arXiv:2409.00204 (2024).
- [29] J. Xu, H. Ren, S. Cai, X. Zhang, An improved faster r-cnn algorithm for assisted detection of lung nodules, Computers In Biology And Medicine 153 (2023) 106470.
- [30] Y. Su, D. Li, X. Chen, Lung nodule detection based on faster r-cnn framework, Computer Methods and Programs in Biomedicine 200 (2021) 105866.
- [31] C. Tong, B. Liang, M. Zhang, R. Chen, A. K. Sangaiah, Z. Zheng, T. Wan, C. Yue, X. Yang, Pulmonary nodule detection based on isodata-improved faster rcnn and 3d-cnn with focal loss, ACM Transactions on Multimedia Computing, Communications, and Applications (TOMM) 16 (1s) (2020) 1–9.
- [32] N. Venkateswarlu, P. Raju, Fast isodata clustering algorithms, Pattern recognition 25 (3) (1992) 335–342.
- [33] X. Wu, H. Zhang, J. Sun, S. Wang, Y. Zhang, Yolo-msrf for lung nodule detection, Biomedical Signal Processing and Control 94 (2024) 106318.
- [34] Z. Ji, J. Zhao, J. Liu, X. Zeng, H. Zhang, X. Zhang, I. Ganchev, Elct-yolo: an efficient one-stage model for automatic lung tumor detection based on ct images, Mathematics 11 (10) (2023) 2344.
- [35] Z. Zhang, K. A. Ahmed, M. R. Hasan, T. Gedeon, M. Z. Hossain, A deep learning approach to diabetes diagnosis, in: Asian Conference on Intelligent Information and Database Systems, Springer, 2024, pp. 87–99.
- [36] J. Hu, L. Shen, G. Sun, Squeeze-and-excitation networks, in: Proceedings of the IEEE conference on computer vision and pattern recognition, 2018, pp. 7132–7141.
- [37] S. Woo, J. Park, J.-Y. Lee, I. S. Kweon, Cbam: Convolutional block attention module, in: Proceedings of the European conference on computer vision (ECCV), 2018, pp. 3–19.
- [38] Q.-L. Zhang, Y.-B. Yang, Sa-net: Shuffle attention for deep convolutional neural networks, in: ICASSP 2021-2021 IEEE International Conference on Acoustics, Speech and Signal Processing (ICASSP), IEEE, 2021, pp. 2235–2239.
- [39] Y. Liu, Z. Shao, Y. Teng, N. Hoffmann, Nam: Normalization-based attention module, arXiv preprint arXiv:2111.12419 (2021).
- [40] Q. Hou, D. Zhou, J. Feng, Coordinate attention for efficient mobile network design, in: Proceedings of the IEEE/CVF conference on computer vision and pattern recognition, 2021, pp. 13713–13722.
- [41] Q. Wang, B. Wu, P. Zhu, P. Li, W. Zuo, Q. Hu, Eca-net: Efficient channel attention for deep convolutional neural networks, in: Proceedings of the IEEE/CVF conference on computer vision and pattern recognition, 2020, pp. 11534–11542.
- [42] X. Wang, R. Girshick, A. Gupta, K. He, Non-local neural networks, in: Proceedings of the IEEE conference on computer vision and pattern recognition, 2018, pp. 7794–7803.
- [43] P. Veličković, G. Cucurull, A. Casanova, A. Romero, P. Lio, Y. Bengio, Graph attention networks, arXiv preprint arXiv:1710.10903 (2017).
- [44] J. Park, S. Woo, J.-Y. Lee, I. S. Kweon, Bam: Bottleneck attention module, arXiv preprint arXiv:1807.06514 (2018).
- [45] Z. Huang, X. Wang, L. Huang, C. Huang, Y. Wei, W. Liu, Ccnet: Criss-cross attention for semantic segmentation, in: Proceedings of the IEEE/CVF international conference on computer vision, 2019, pp. 603–612.
- [46] T. Dai, J. Cai, Y. Zhang, S.-T. Xia, L. Zhang, Second-order attention network for single image super-resolution, in: Proceedings of the IEEE/CVF conference on computer vision and pattern recognition, 2019, pp. 11065–11074.
- [47] A. V. EGA, W. ARDIATNA, Study on image processing method and data augmentation for chest x-ray nodule detection with yolov5 algorithm, ELKOMIKA: Jurnal Teknik Energi Elektrik, Teknik Telekomunikasi, & Teknik Elektronika 11 (2) (2023) 424.
- [48] L. Goel, P. Patel, Improving yolov6 using advanced pso optimizer for weight selection in lung cancer detection and classification, Multimedia Tools and Applications (2024) 1–34.
- [49] S. Mameri, M. Amroune, M.-Y. Haouam, I. Bendib, A. Corrêa Silva, Early detection and diagnosis of lung cancer using yolo v7, and transfer learning, Multimedia Tools and Applications 83 (10) (2024) 30965–30980.
- [50] C. Şaman, Ş. Çelikbaş, Yolov8-based lung nodule detection: A novel hybrid deep learning model proposal, International Research Journal of Engineering and Technology 10 (8) (2023) 230–237.
- [51] S. Jain, P. Choudhari, M. Gour, Pulmonary lung nodule detection from computed tomography images using two-stage convolutional neural network, The Computer Journal 66 (4) (2023) 785–795.
- [52] H. Zhang, H. Zhang, Lungseek: 3d selective kernel residual network for pulmonary nodule diagnosis, The Visual Computer 39 (2) (2023) 679–692.
- [53] H. Lu, K. Liu, H. Zhao, Y. Wang, B. Shi, Dual-layer detector spectral ct-based machine learning models in the differential diagnosis of solitary pulmonary nodules, Scientific Reports 14 (1) (2024) 4565.
- [54] M. Tan, R. Pang, Q. V. Le, Efficientdet: Scalable and efficient object detection, in: Proceedings of the IEEE/CVF conference on computer vision and pattern recognition, 2020, pp. 10781–10790.
- [55] X. Zhou, D. Wang, P. Krähenbühl, Objects as points, arXiv preprint arXiv:1904.07850 (2019).
- [56] K. Liu, Stbi-yolo: A real-time object detection method for lung nodule recognition, IEEE Access 10 (2022) 75385–75394.
- [57] Z. Ji, Y. Wu, X. Zeng, Y. An, L. Zhao, Z. Wang, I. Ganchev, Lung nodule detection in medical images based on improved yolov5s, IEEE Access (2023).

APPENDIX

DETAILED ANALYSIS OF TRAINING PROGRESS

The training curves shown in Figure 12 compare the performance of the MSDet model against YOLOv3, YOLOv7, Scaled_YOLOv4, and TPH-YOLOv5 across 200 epochs using metrics such as mAP_{0.5} and mAP from 0.5 to 0.95. MSDet demonstrates rapid convergence and superior performance, achieving a 60% mAP at 0.5 to 0.95 by epoch 125, highlighting its efficient learning and adaptation capabilities.

The graph presents key metrics including mAP at IoU 0.5, mAP from 0.5 to 0.95, precision, and recall. These metrics illustrate MSDet’s consistently higher precision and recall, maintaining smooth and stable progress. The model’s early high performance, especially in mAP at IoU 0.5, underscores its effective adaptation to complex image data with fewer epochs compared to other models. This enhanced performance is due to MSDet’s sophisticated feature extraction and optimized learning strategies.

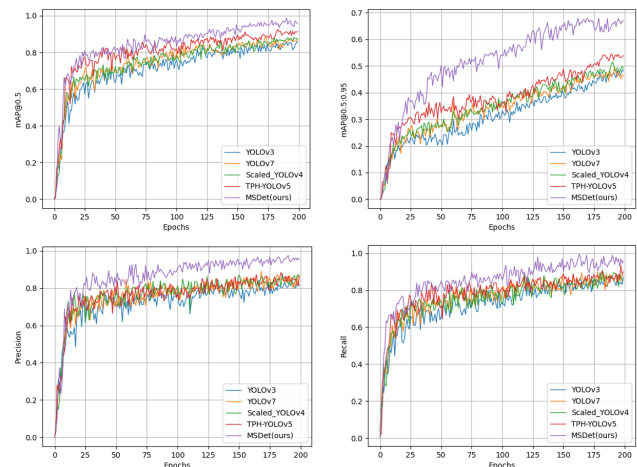


Fig. 12. Training performance comparison of MSDet with YOLO variants across 200 epochs. The graph demonstrates MSDet’s superior performance with a clear lead in mAP scores from IoU 0.5 to 0.95, underscoring its rapid convergence and higher accuracy in detecting more complex features effectively.